CLM - P 47

United Kingdom Atomic Energy Authority

RESEARCH GROUP

Preprint

DIFFUSION OF TRAPPED REVERSED MAGNETIC FIELD IN A THETA PINCH IN THE PRESENCE OF A PROBE

M. KEILHACKER

Culham Laboratory,

Culham, Abingdon, Berkshire

1964

UNCLASSIFIED
(Approved for Publication)

CLM - P 47

DIFFUSION OF TRAPPED REVERSED MAGNETIC FIELD IN A THETA PINCH IN THE PRESENCE OF A PROBE*

by

M. KEILHACKER

(Submitted for publication in Nuclear Fusion)

ABSTRACT

The trapped reversed flux in a 26 kJ Theta Pinch with known initial conditions is measured as a function of time with a radial multiple probe and compared with numerical calculations. The measured flux agrees with the numerical calculations during the implosion of the plasma but decreases rapidly after the maximum compression whereas the calculated flux remains almost constant because of the increasing plasma temperature.

It is shown that radiation cooling by probe impurities can explain this enhanced field diffusion in the neighbourhood of the probe. The numerical calculations can be fitted to the experimental results by increasing the radiation loss due to hydrogenic continuum radiation by a few times 10^4. It is estimated that the heat flow to the probe, which is mainly carried by ions (with an energy according to the floating potential of the probe) liberates enough oxygen to account for this factor due to line radiation. Radial framing camera photographs show a tearing mode resistive instability developing near the probe which seems to be started off by this radiation cooling.

A limit on the reliability of probe measurements is given as a function of plasma density and temperature.

*Work performed as part of the joint research programme of the Institut für Plasma Physik, Garching, and Euratom

U.K.A.E.A. Research Group,
Culham Laboratory,
Nr. Abingdon,
Berks.

June, 1964
(C/18 IMG)

CONTENTS

1. Introduction

Probe measurements of the magnetic field in a Theta Pinch plasma with trapped reversed field often show (Fig.2b) a 'break-through' of the driving magnetic field into the plasma[1,2,3,4,5] which cannot be explained by classical field diffusion in a pure plasma. It has long been suspected [1,2] - and was recently verified for the SCYLLA I Theta Pinch [6] - that this field break-through is caused by the probe itself which is eroded by the hot plasma and emits impurities which cool the plasma. Apart from this effect the external magnetic field usually even without a material probe breaks through faster than predicted by theory. This is probably caused by axial contraction and/or by resistive instabilities.

The following paper presents a study of this subject. Probe measurements of the radial magnetic field distribution in a Theta Pinch with known initial conditions (electron density and temperature, amplitude of trapped reversed field) are compared with numerical calculations based on the hydromagnetic equations for a fully ionized plasma (see section 3). It is shown that the measured rate of change of trapped reversed flux agrees with the numerical calculations up to the first maximum compression and electron temperatures are derived from the diffusion time using a simple model (see section 4a). After the first maximum compression the probes indicate an increased diffusion of the magnetic field whereas the numerical calculations show the diffusion slowing down due to the increasing plasma temperature. This enhanced field diffusion can be explained by line radiation cooling from probe impurities if their concentration in the immediate neighbourhood of the probe exceeds 50% (see section 4b). Section 4c gives estimates which show that the heat flow (by radiation and ions) to the probe boils off enough probe material in a tenth of a microsecond to account for this impurity concentration.

2. Experimental Arrangement

The experiments were carried out with the 26 kJ Theta Pinch II at Garching described previously [7]. The main discharge which produced a peak field of 53kG and a half period of 3.1 μsec in a coil of 30 cm length and 5.4 cm diameter was

fired into an almost completely ionized plasma (fast Theta pinch preionization) which contained a trapped bias magnetic field, B_{zo}($-$ 2.5 kG $\leqslant B_{zo} \leqslant$ 2.5 kG). The filling gas was hydrogen at a pressure of 0.10 or 0.15 torr. A bakeable quartz discharge tube was used. The base pressure was of the order 10^{-6} torr. The impurity concentration has been determined spectroscopically [7]. Oxygen, the greatest impurity, was less than 0.2% in the preionization but increased to about 1% at the beginning of the main discharge. Carbon was less than 0.02% in the main discharge.

The radial magnetic field distribution in the centre plane of the coil was measured with a multiple magnetic probe consisting of six pick-up loops, spaced radially 2.5 mm apart from each other (Fig.1). Each pick-up loop consisted of 20 turns of 0.045 mm copper wire on a 0.8 mm diameter tephlon core. The loops were electrostatically shielded by a mesh of fine copper wire and their leads were run in a brass tube of 1.5 mm O/D. The moveable probe was protected from plasma by a quartz jacket of 2.5 mm O/D which formed part of the discharge tube (Fig.1).

3. Radial Magnetic Field Distribution

Fig.2a shows a typical set of radial magnetic field distributions at various points of time (dotted lines) which have been evaluated from the probe signals. The corresponding points of time are indicated by arrows on the probe signal of Fig.2b which shows the magnetic field on the discharge axis.

The measured field distributions are compared with theoretical values (solid lines) which are based on the numerical solution of the hydromagnetic equations for a fully ionized plasma in Theta Pinch geometry as described in [8,9,10]. The boundary conditions were the same as those described in [8] except that the circuit details were eliminated and the external field B was given by the form

$$B = B_o \exp(-\delta t) \sin \frac{2\pi}{T} (t - \varepsilon).$$

The parameters B_o = 56 kG, $\delta = 5.7 \times 10^4$ s^{-1} and T = 6.2 μsec were chosen to correspond with the experimental conditions. The quantity ε was adjusted to

make the external field equal to the trapped field at the beginning of the numerical calculations [10].

In order to start the numerical calculation with the appropriate initial conditions electron density and electron temperature in the pre-ionization were measured spectroscopically as described in [7]. Electron and ion temperature were assumed to be equal. The trapped magnetic field was measured with probes.

Fig.2a shows that the measured field distribution agrees quite well with the theoretical one up to the first maximum compression at 0.3 μsec. Measured field gradients are smaller than the theoretical ones which can be explained by the incomplete ionization at the beginning of the main discharge. After the first maximum compression the measured trapped field decreases rapidly and the external magnetic field diffuses into the plasma core whereas the numerical calculations show several compressions of the reversed field which remains trapped because of the increasing temperature. This discrepancy is analysed in more detail in the next section.

4. Decrease of Trapped Reversed Flux

The trapped reversed flux, Φ, as a function of time, t

$$\Phi(t) = 2\pi \int_0^{r(t)_{B=0}} B(r,t)\,r\,dr \qquad r(t)_{B=0} = \text{radius of } B=0 \text{ surface}$$

was calculated from the measured radial field distribution $B(r,t)$ for three discharges with different initial gas pressure p_o, temperature T_o and amplitude of trapped reversed field B_{zo}. The results are plotted in Fig.3 (dotted lines) in relative units $\Phi(t)/\Phi_o$, where $\Phi_o = B_{zo}\,\pi\,r_o^2$ is the initially trapped flux. The relative experimental error (i.e. the error in $\Phi(t)$) is less than 15%, the total experimental error (i.e. including errors in Φ_o) less than 25%.

The experimental result is compared with numerical values (solid lines). They were computed for each of the three discharges using the corresponding measured

initial values. This was necessary because the decrease of trapped flux during the first implosion depends on the initial values of temperature and trapped field. This is shown in Fig.4 where these quantities are varied in a set of numerical runs.

(a) 'Normal' Field Diffusion during Implosion

The comparison between measured and theoretically predicted decrease of flux in Fig.3 shows that up to the first maximum compression the agreement is very good for both cases at 0.10 torr which started in an almost fully ionized plasma (T_o = 1.5 and 2 eV respectively). At 0.15 torr the plasma was only 30% preionized (T_o = 1 eV) and therefore the flux decreases somewhat faster than predicted by the fully ionized programme*.

The good agreement indicates that up to the first maximum compression the probe does not affect the plasma and that the field measured by the probe is reliable. The electron temperature T_e was therefore estimated from the rate of change of flux using a simple model which has previously been described in [12]. If the time for field to diffuse across the plasma annulus with thickness Δ is small compared with the time in which the plasma parameters change, the rate of change of trapped reversed flux can be described by the equation

$$\frac{d(\pi\, r^2\, B_t)}{dt} = 2\,\pi r\, v_d\, (B_e - B_t)\ , \qquad \ldots (1)$$

where $v_d = \eta/4\pi\Delta$ is a diffusion velocity of the field into the plasma. Using Spitzer's formula [13] for the plasma resistivity η one gets the following equation for T_e

$$\frac{d\Phi}{dt} = \frac{r(B_e - B_t)}{2\Delta} \cdot \frac{6.53 \times 10^{12}\ \ell n\Lambda}{T_e^{3/2}}\ , \qquad \ldots (2)$$

in which all other quantities are determined by the measured field distribution. Fig.5 shows the electron temperatures T_e (solid lines) during the first implosion

---

* A preliminary comparison with numerical calculations using a partially ionized programme [11] shows good agreement.

calculated by this method*. There is a good fit with the initial temperatures T_{eo} (points at $t = 0$), which have been measured in the preionization, and rise to 20 - 40 eV at the first maximum compression in good agreement with the numerical calculations. However, near the compression maximum the possible error in these calculations is rather high because of the small slope in the experimental $d\Phi/dt$ curves (Fig.3).

Fig.5 also shows the diffusion velocity v_d (dotted lines) calculated from the measured quantities using equation (1). The diffusion velocity slows down during the implosion but after the maximum compression it increases by an order of magnitude.

(b) 'Enhanced' Field Diffusion after First Compression due to Impurity Radiation Losses

In contrast to the good agreement between measured and theoretically predicted field diffusion during the implosion the results after the compression show a striking discrepancy (Fig.3). The trapped reversed flux measured by the probes decreases rapidly and vanishes at about 0.5 μsec while the numerical calculations indicate a continuously decreasing rate of change of flux due to the increasing plasma temperature and reversed flux remains trapped during the whole half-cycle (3 μsec). This enhanced field diffusion must result from an increase in plasma resistivity either due to an instability or because of an anomalous drop in plasma temperature.

The plasma stability has been studied by means of radial stereoscopic framing camera photographs. In order not to perturb the plasma near the probe only a 10 cm section at one end of the 30 cm coil was slotted. The photographs (Fig.6) up to 0.4 μsec show a stable hollow plasma cylinder with a non luminous core of trapped flux. The plasma column then contracts axially, the dark core remaining

---

* For $\ell n\Lambda$ values between 6 and 10 have been used according to measured electron densities [5] and calculated electron temperatures (using equation (2) in an iteration).

in the outer part of the coil but disappearing near the median plane (probe region) where the plasma contracts radially and disintegrates at about 1 μsec. This indicates that the external magnetic field first breaks through near the probe, thereby dividing the hollow plasma cylinder into two parts each of which contracts axially. This process can be regarded as a tearing mode resistive instability [14] which is started off by radiation cooling from probe impurities.

In order to examine quantitatively the influence of increased radiation on the field diffusion, numerical calculations were carried out in which the term representing the radiation loss due to hydrogenic continuum radiation was suddenly increased by a constant factor, R, after 0.2 or 0.3 μsec respectively. R was varied between 10 and 10^5. The results (Fig.7) demonstrated that the calculations can be fitted to the experimental points by increasing the radiation loss by a factor of 3×10^4 to 10^5, which reduces the mean plasma temperatures from about 50 eV at 0.3 μsec to about 10 eV at 0.45 μsec. As the continuum radiation is proportional to the square of the density, the plasma temperature drops most rapidly in the high density plasma layer which separates the external magnetic field from the trapped field. In order to maintain pressure balance the plasma density in this region rises, which again increases the radiation loss. This process is shown in Fig.8 where the calculated distributions of T_e, N_e and B_z for the normal case of $R = 1$ (solid lines) are compared with those for which $R = 3 \times 10^4$ for $t \geqslant 0.2$ μsec (dotted lines). In the experiment the fall in temperature and the increase in density will not be so pronounced as self-absorption of the radiation reduces the radiation losses.

Bremsstrahlung from impurities, which is higher by a factor Z^2 than hydrogenic Bremsstrahlung cannot account for a factor of 10^4 ($Z^2 = 36$ for O VI). But incompletely stripped impurity ions, which become excited by collisions with electrons, and decay subsequently, produce line radiation which is some orders of magnitude higher [15,16,17]. An approximate calculation in [16] shows that under conditions where a steady-state is reached (this is in 0.1 μsec for O VI at $N_e = 10^{17}$ cm^{-3} and $T_e = 50$ eV) and where no self-absorption occurs the line

radiation of O VI is 2×10^4 times the hydrogenic Bremsstrahlung at 50 eV. This ratio increases at lower temperatures. Thus the impurity concentration around the probe must be at least 50% of the total particle density in order to increase the radiation by a few times 10^4. 50% represents a lower limit because the radiation will be reduced by self-absorption at these high impurity densities.

(c) Probe as Source of Impurities

It will now be estimated whether the heat flux to the quartz jacket is likely to raise the quartz surface above its vaporization point in 10^{-7} sec* and thereby produces a high impurity concentration around the probe. To do this one has to solve the thermal diffusion equation for the quartz wall

$$\frac{\partial T}{\partial t} = \frac{\lambda}{\rho c} \cdot \frac{\partial^2 T}{\partial t^2} \quad , \qquad \ldots (3)$$

where ρ = density, c = specific heat, and λ = thermal conductivity, together with the appropriate boundary conditions

$$T = 0 \quad \text{at} \quad t = 0$$

and

$$q = -\lambda \left(\frac{\partial T}{\partial x}\right)_{x = 0} \quad , \qquad \ldots (4)$$

where q = heat flux density.

The solution of equation (3) together with equations (4) for constant heat flux q is [20]

$$T(x,t) = \frac{q}{\lambda}\left[2\sqrt{\frac{Kt}{\pi}} \cdot \exp\left(-\frac{x^2}{4Kt}\right) - x \cdot \operatorname{erfc}\left(\frac{x}{2\sqrt{Kt}}\right)\right] , \qquad \ldots (5)$$

where $\operatorname{erfc}(x/2\sqrt{Kt}$ has the usual meaning of 'complementary error function' of $x/2\sqrt{Kt}$ and $K = \lambda/c\rho$ = diffusivity. Therefore the temperature at the quartz surface $x = 0$ is

$$T(0,t) = 2q\sqrt{\frac{t}{\pi c \rho \lambda}} \quad , \qquad \ldots (6)$$

and the depth of penetration of heat into the quartz, d, is approximately

---

* The question of wall evaporation in pulsed gas discharges has also been investigated in [18] and [19] .

(neglecting the second term in equation (5))

$$d = 2\sqrt{Kt} \qquad \ldots (7)$$

Now the heat flux density, q, will be estimated. Let us first consider the heat flux q_i carried by ions. It consists of their kinetic energy and their ionization energy which is released as they are neutralised at the quartz surface. The kinetic energy of the ions is $e \cdot U_f$, where U_f is the negative 'floating potential' of the quartz surface caused by the fact that more electrons than ions flow to the quartz surface. U_f is determined by the condition that in equilibrium electron and ion flow must be equal and is [21]

$$U_f = \frac{k\,T_e}{e}\ \ell n\ (0.658\sqrt{m_i/m_e}\ ) \ . \qquad \ldots (8)$$

For a hydrogen plasma

$$U_f = 2.9 \times 10^{-4}\ T_e \ \text{Volt} \ , \qquad \ldots (8')$$

if T_e is measured in ^oK. The flux of ions is $\frac{1}{4}\, n_i v_i$, where n_i = ion density (cm^{-3}) and $v_i = \sqrt{3\ k\ T_i/m_i}$ = average ion velocity. The heat flux density, q_i, is therefore

$$q_i = \tfrac{1}{4}\, n_i\, v_i\, (e\, U_f + e\, U_i) \ , \qquad \ldots (9)$$

where U_i = ionization potential. Substituting equation (8) in equation (9) and setting $T_e = T_i = T\ (^oK)$ one gets in a hydrogen plasma for $T > 5 \times 10^4\ ^oK$ (i.e. neglecting U_i against U_f in equation (9))

$$q_i = 1.8 \times 10^{-19}\ n_i\ T^{3/2}\ \ W/cm^2 \ . \qquad \ldots (9')$$

For typical experimental conditions of $n = 10^{17}\ cm^{-3}$ and $T = 2 \times 10^5\ ^oK$ or $5 \times 10^5\ ^oK$ respectively on gets $q_i = 2\ MW/cm^2$ or $7.5\ MW/cm^2$ respectively.

The radiative heat flux, q_r, due to line radiation from impurities is rather difficult to calculate as self-absorption has to be considered. The effect of self-absorption can be regarded as to convert a spectral line into a rectangular emission spectrum with a 'line' width $\Delta\nu_o$ determined by the points in the spectrum where $k(\nu) \cdot a \approx 1$ (where $k(\nu)$ = absorption coefficient and a = plasma depth) and a maximum amplitude given by the black body value, $B_{\nu o}$. The amplitude

is smaller than $B_{\nu o}$ if the radiation is non thermal [17]. The radiation emitted by a single line is therefore

$$q_r \leqslant B_{\nu o}\, \Delta\nu_o \quad \text{with} \quad B_{\nu o} = \frac{2\pi h \nu^3}{c^2(\exp h\nu/kT - 1)} \qquad \ldots (10)$$

For a simplified model in which the plane probe surface receives radiation from a plasma slab of thickness a one gets for the 'line' width (using the deduction in [16], except for change in geometry)

$$\Delta\nu_o = 350\, n_{io}^{\frac{1}{2}}\, a^{\frac{1}{2}} \left(\frac{g_2}{g_1}\right)^{\frac{1}{2}} \left(1 + \frac{\gamma_\rho}{\gamma}\right)^{\frac{1}{2}} \ s^{-1}\ , \qquad \ldots (11)$$

where n_{io} = number of ions in ground state (cm^{-3}), a = plasma thickness (cm) γ = spontaneous emission probability of excited ions (s^{-1}), γ_ρ = effective de-excitation collision frequency between excited ion and the surrounding plasma particles (s^{-1}) and g_2/g_1 = ratio of statistical weights of the two states. Substituting equation (11) in equation (10) and assuming $h\nu/kT \ll 1$ one gets for the heat flux radiated by a single impurity line

$$q_r \leqslant 3 \times 10^{-41}\, \nu^2\, T\, n_{io}^{\frac{1}{2}}\, a^{\frac{1}{2}} \left(\frac{g_2}{g_1}\right)^{\frac{1}{2}} \left(1 + \frac{\gamma_\rho}{\gamma}\right)^{\frac{1}{2}} \ W/cm^2 \qquad \ldots (12)$$

As an example the heat flux radiated by the $2S - 2P$ resonance line of O VI will be estimated for which $\lambda = 1032$ Å (i.e. $\nu = 3 \times 10^{15}\ s^{-1}$), $g_2/g_1 = 2$, $\gamma = 4 \times 10^8\ s^{-1}$ and $\gamma_\rho = 6 \times 10^8\ s^{-1}$ (calculated from tables in [22]). To get an upper limit rather high values $n_{io} = 10^{17}\ cm^{-3}$, $T = 5 \times 10^5\ ^oK$ and $a = 1$ cm will be assumed. Then equation (12) gives $q_r \leqslant 7 \times 10^4\ W/cm^2$.

This shows that under these experimental conditions the radiative heat flux is two orders of magnitude smaller than the heat flux carried by ions.

Using the estimated values of the heat flux, q, and replacing $T(0,t)$ by the melting point of quartz, T_m, equation (6) gives the time t_{mo} at which the quartz surface melts and quartz material is likely to be involved in the discharge. Substituting t_{mo} in equation (7) we get the depth d_m at which the temperature has dropped to about $\frac{1}{e} T_m$ at time t_{mo}. The time it takes to melt the material at this depth d_m is approximately $t_{md} = e^2\, t_{mo}$ (neglecting the second term in

equation (5)). The latent heat need not be included in these estimates as it consumes only about 5% of the energy.

Table 1 shows these quantities for different values of the heat flux, q, using T_m = 1700 °C, ρ = 2.2 g/cm³, $\bar{c}$ = 0.28 cal/g °C and $\bar{\lambda}$ = 0.8 × 10^{-2} cal/cm s °C, where $\bar{c}$ and $\bar{\lambda}$ are approximate mean values between 0 and 1700 °C. The result shows that at the expected heat flux of a few MW/cm² the quartz surface is heated to its melting point in about 10^{-8} s and in about 10^{-7} s a quartz layer of a few times 10^{-5} cm is boiled off.

Table 1

Onset time of quartz evaporation, t_{mo}, and thickness of quartz layer, d_m, which is likely to be boiled off in a time t_{md} for different values of heat flux density, q

q (MW/cm²)	t_{mo} (μs)	t_{md} (μs)	d_m (cm)
0.1	20	150	10^{-3}
1	0.2	1.5	10^{-4}
10	0.002	0.015	10^{-5}

Assuming that the emitted oxygen atoms are homogeneously distributed around the probe their density (cm^{-3}) as a function of time is

$$n_O(t) = \frac{2\, N_O\, r_o\, x_m(t)}{[r_o + \bar{v}(t - t_{mo})]^2 - r_o^2}\,, \qquad \ldots (13)$$

where N_O = oxygen density in quartz ≈ 5 × 10^{22} cm^{-3}, $\bar{v}$ = mean thermal velocity of the oxygen ions, r_o = probe radius = 0.125 cm and $x_m(t)$ = depth of quartz layer (cm) with $T = T_m$, to be calculated from equation (5). In first approximation $x_m(t)$ is proportional to $(t)^{+\frac{1}{2}}$ and the oxygen density $n_O(t)$ decreases with $(t)^{-\frac{1}{2}}$ for $t < 2r_o/\bar{v}$ and with $(t)^{-\frac{3}{2}}$ for $t > 2r_o/\bar{v}$.

Using equations (13) and (5) one gets at a heat flux density of a few MW/cm² (this value is to be expected at the first maximum compression) an oxygen density

of 6×10^{18} cm^{-3} for $t = 0.1$ μsec and of 1×10^{18} cm^{-3} for $t = 0.5$ μsec, the impure plasma region extending to about 0.2 cm and 1 cm from the probe respectively. This estimate indicates that at the maximum compression the oxygen density near the probe is an order of magnitude higher than the hydrogen density and that these oxygen impurities are very likely to cause the observed field break-through by radiation cooling.

5. Conclusions

The results indicate that in a high density, high temperature plasma probe measurements are limited by the heat flux carried by ions to the probe and evaporating the probe surface. One can deduce an approximate limit for the time of undisturbed observation, t_{obs}, by setting it equal to the time t_{mo} it takes to melt the probe surface. For a quartz probe in a hydrogen plasma one gets from equations (6) and (9)

$$t_{obs} \approx t_{mo} = 6 \times 10^{42} \; n_i^{-2} \; T^{-3} \; , \qquad \ldots (14)$$

where n_i is measured in cm^{-3} and T in ^{o}K.

For $n_i = 5 \times 10^{16}$ cm^{-3} and $T = 10^5$ ^{o}K, which are typical conditions during the implosion phase of a Theta Pinch, $t_{obs} = 0.25$ μsec, but it decreases rapidly as the hot plasma builds up. The probe measurements of the radial magnetic field distribution agree with this picture: they show a normal field diffusion during the implosion phase (up to 0.3 μsec) but a break-through of the external magnetic field near the probe after the maximum compression which can be explained by radiation cooling from probe impurities.

6. Acknowledgements

I gratefully acknowledge the co-operation of Dr. A. Eberhagen in carrying out the experiments.

I wish to thank Mr. D.L. Fisher for his contribution of the numerical calculations and Dr. H.A.B. Bodin, Dr. G.B.F. Niblett and Dr. J.A. Reynolds for many helpful discussions.

7. References

1. K. BOYER et al., Phys. Rev., 119, 831, (1960)

2. H.R. GRIEM et al., Nucl. Fusion 1962 Suppl., Pt.2, 543

3. E. HINTZ, Nucl. Fusion 1962 Suppl., Pt.2, 601

4. E. FÜNFER et al., Z. Naturforschg., 17a, 967 (1962)

5. A. EBERHAGEN and M. KEILHACKER, Comptes Rendus de la VI^{e} Conference Internationale sur les Phenomenes d'Ionization dans les Gaz, vol.II, 577 (1963)

6. F.C. JAHODA and G.A. SAWYER, Phys. Fluids, 8, 1195, (1963)

7. A. EBERHAGEN and M. KEILHACKER, Comptes Rendus de la VI^{e} Conference Internationale sur les Phenomenes d'Ionization dans les Haz, vol.II, 573 (1963)

8. K. HAIN, Report No. AERE - R 3383, H.M.S.O., (1961)

9. K. HAIN and A. KOLB, Nucl. Fusion 1962 Suppl., Pt.2, 561

10. G.B.F. NIBLETT and D.L. FISHER, Culham Report No. CLM - R 19, H.M.S.O. (1962)

11. D. DÜCHS, Phys. Letters, 5, 121 (1963)

12. J.A. REYNOLDS and N.J. PHILLIPS, Proceedings of the 5th International Conference on Ionization Phenomena in Gases, vol.II, 2288 (1961)

13. L. SPITZER, Jr., Physics of Fully Ionized Gases, p.139, Interscience Publishers, New York (1962)

14. H.A.B. BODIN, Nucl. Fusion, 3, 215 (1963)

15. G. KNORR, Z. Naturforschg., 13a, 941 (1958)

16. R.F. POST, Plasma Dynamics edited by F.H. Clauser, p.30, Pergamon Press, London (1960) and Plasma Physics (Journal of Nuclear Energy Part C), 3, 273 (1961)

17. S. CUPERMAN, F. ENGELMANN and J. OXENIUS, Phys. Fluids, 6, 108 (1963) and Phys. Fluids, 7, 428 (1964)

18. D.E.T.F. ASHBY, Plasma Physics (Journal of Nuclear Energy Part C), 5, 83 (1963)

19. R.A. DUGDALE et al., British Ceramic Soc. Trans., 60, 427 (1961)

20. W.T. THOMSON, Laplace Transformation, p.215, Prentice-Hall, Inc., New Jersey (1960)

21. K. JAMAMOTO and T. OKUDA, J. Phys. Soc. Japan, 11, 57 (1956)

22. C.W. ALLEN, Astrophysical Quantities, The Athlone Press, London (1963)

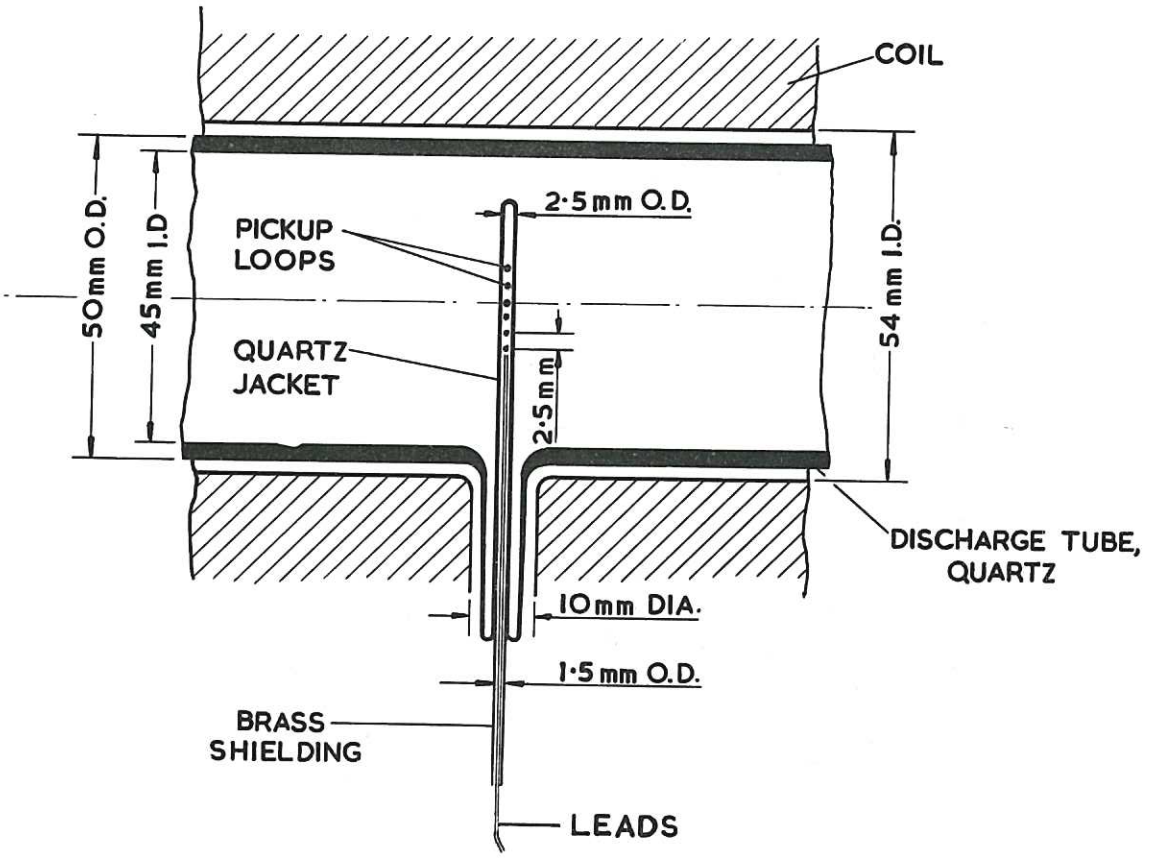

CLM-P47 Fig. 1
Section of discharge tube with radial magnetic probe and quartz jacket

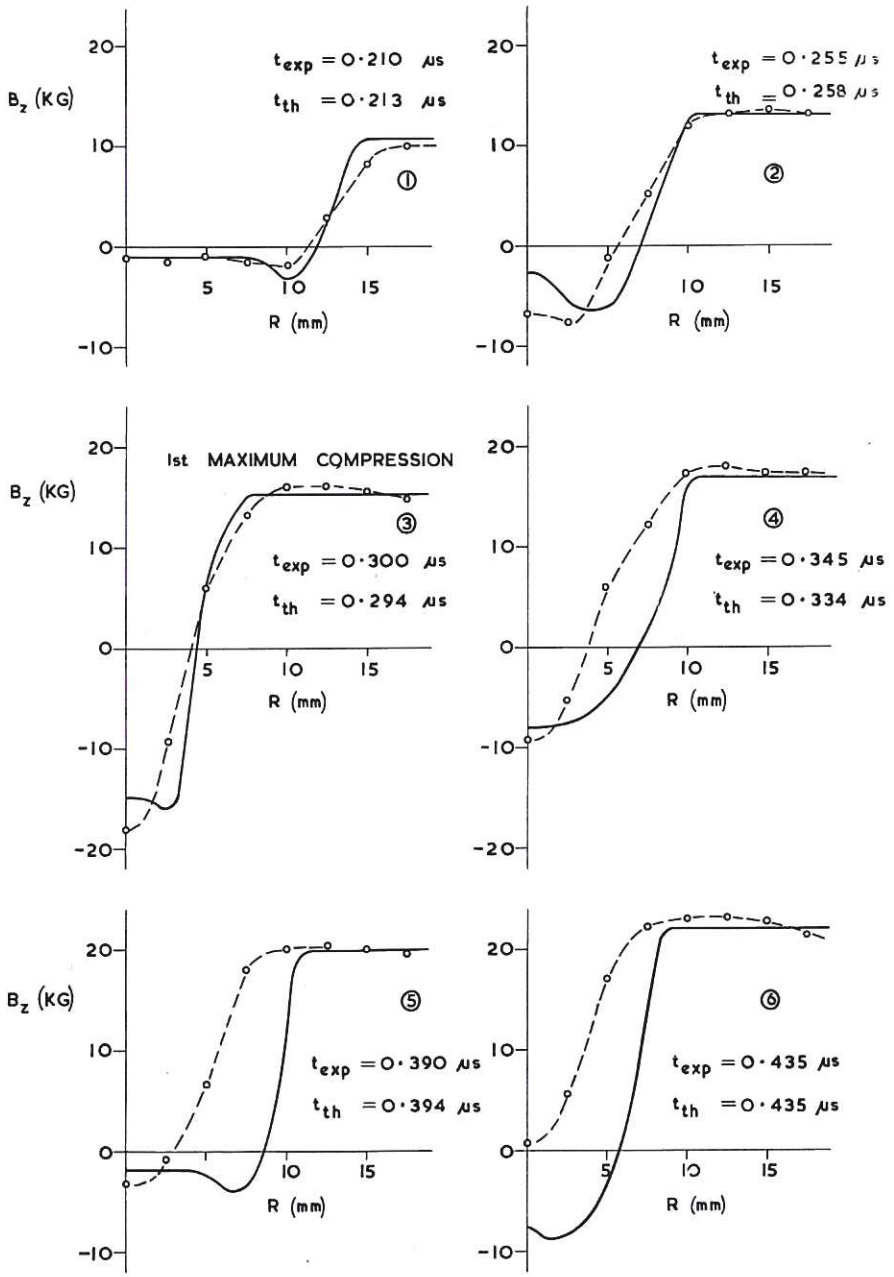

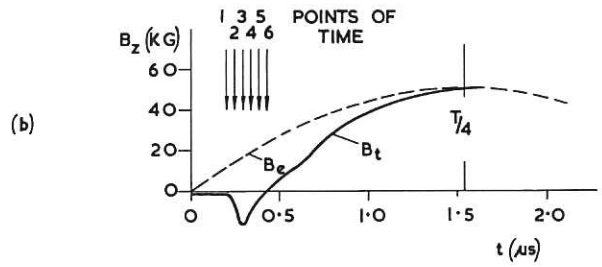

CLM-P 47 Fig. 2

(a) Radial magnetic field distributions, B_z, at different points of time (indicated by arrows in Fig. 2(b))

(b) Probe signal of magnetic field on the axis, B_t, together with external magnetic field, B_e

Initial conditions: p_o = 0.15 torr, T_o = 1 eV, B_{zo} = - 1.4 kG

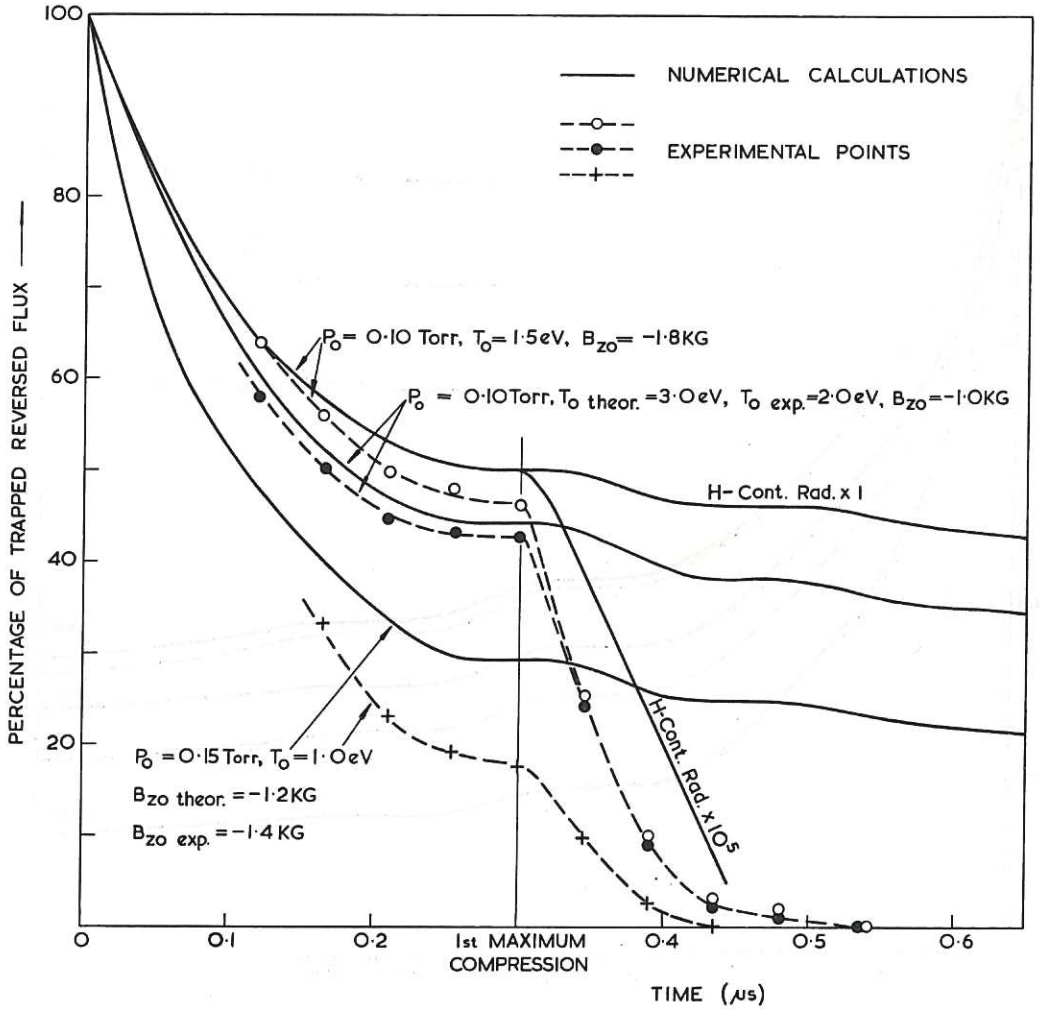

CLM-P 47 Fig. 3

Decrease of trapped reversed flux as a function of time for three sets of initial conditions p_o, T_o and B_{zo}

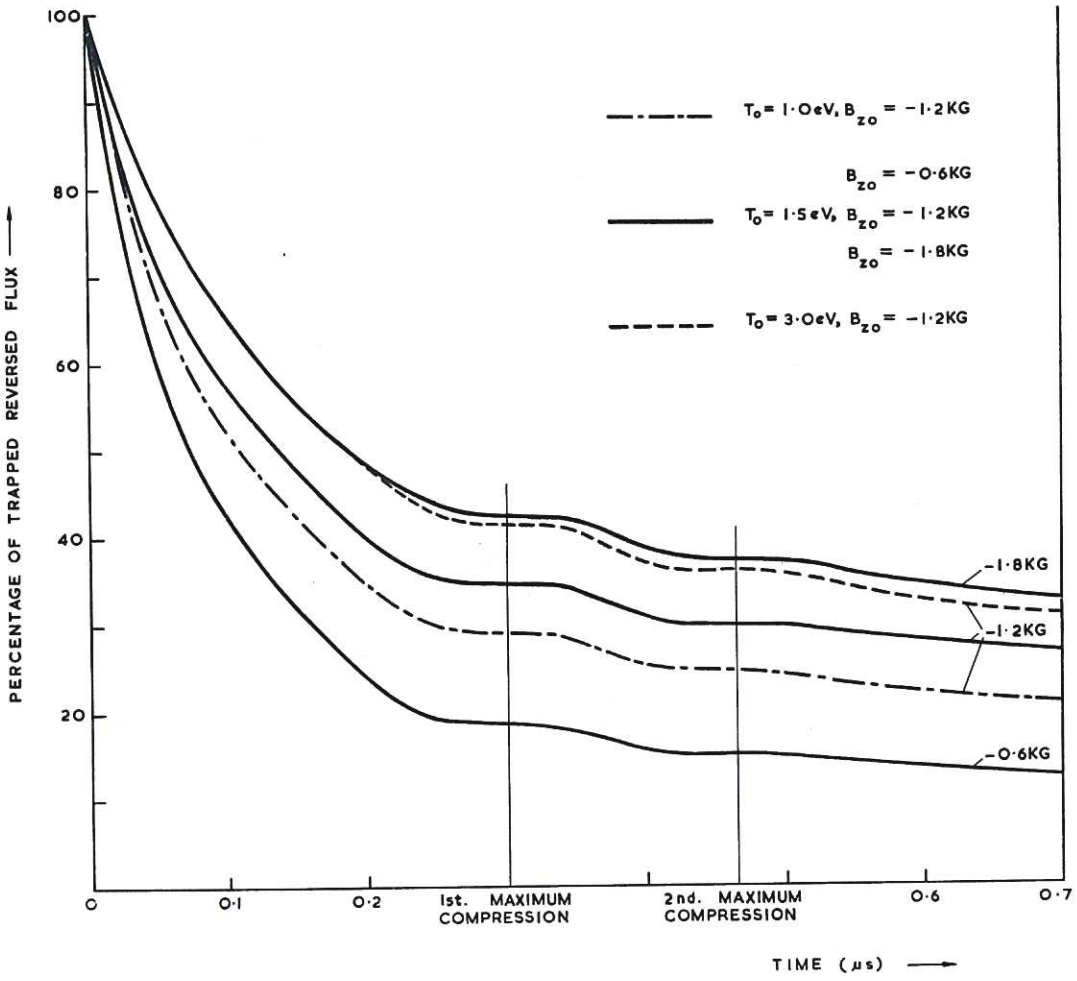

CLM-P 47 Fig. 4

Numerical calculations showing effect of initial temperature, T_o, and amplitude of trapped reversed field, B_{zo}, on decrease of trapped flux.
p_o = 0.10 torr

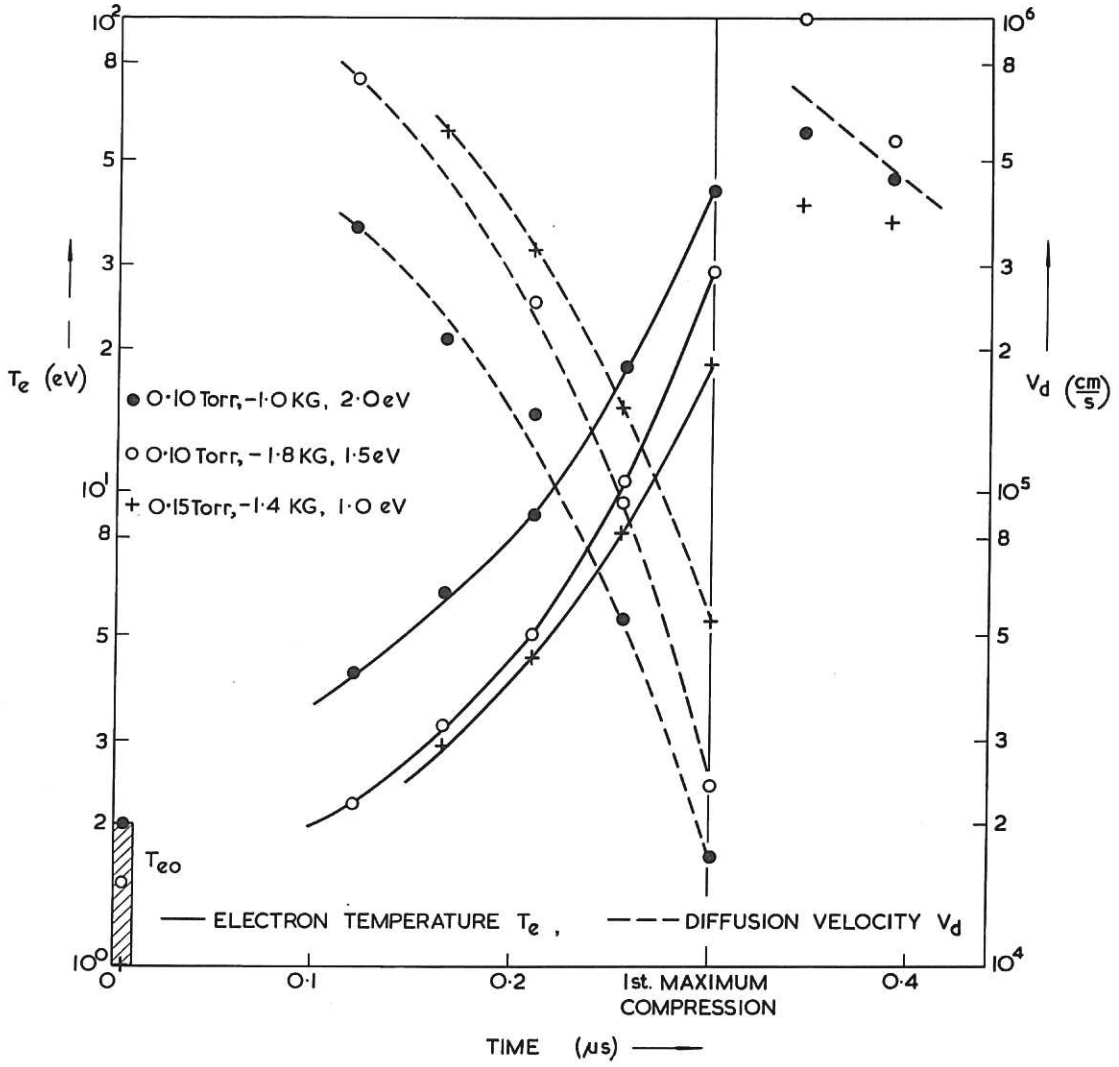

CLM-P 47 Fig. 5

Electron temperature, T_e, and diffusion velocity, v_d, calculated from the measured rate of changed of trapped flux in Fig. 3

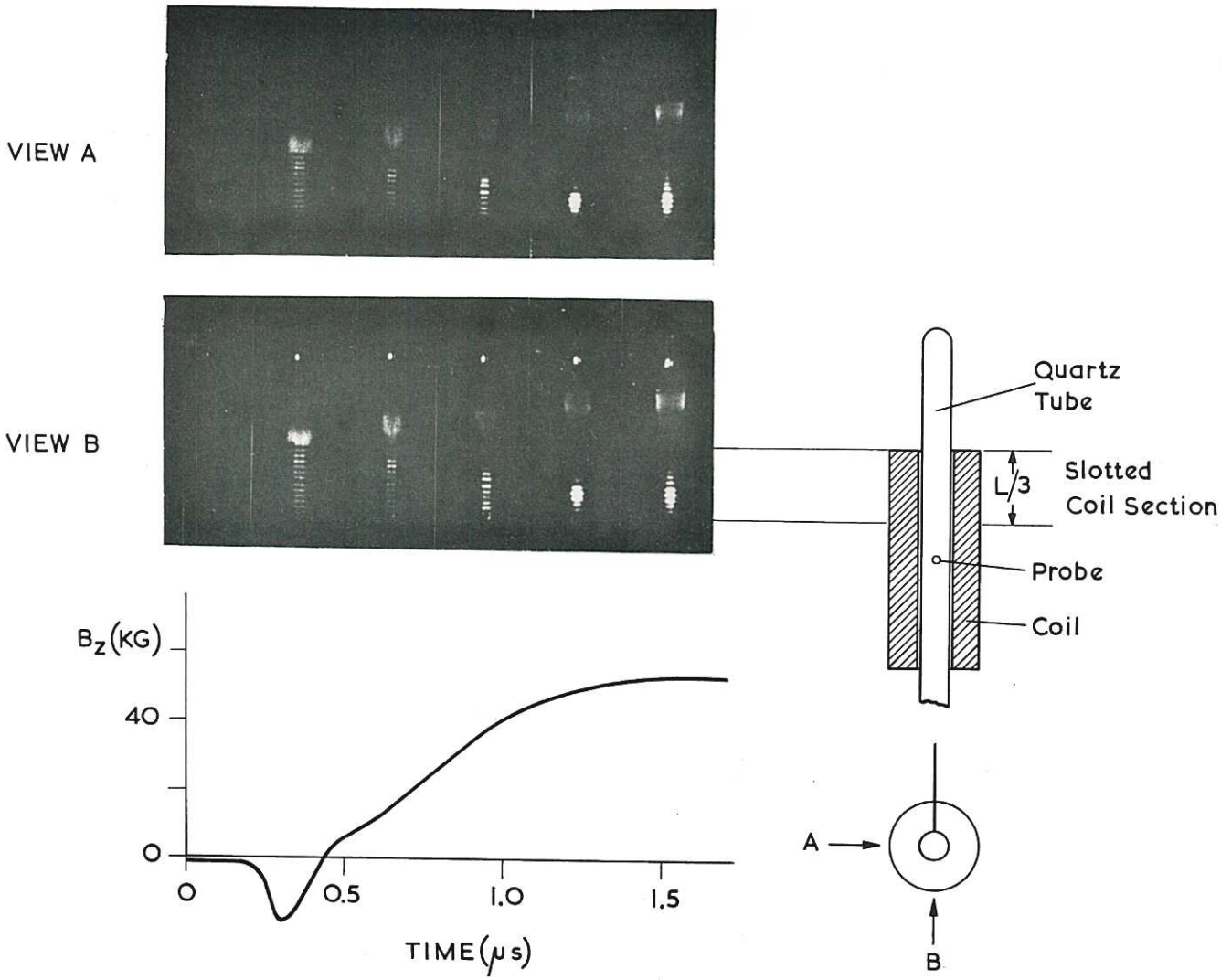

CLM-P47 Fig. 6

Radial stereoscopic framing camera photographs showing axial contraction and disintegration of plasma near probe. $p_o = 0.15$ torr, $B_{zo} = -1.8$ kG

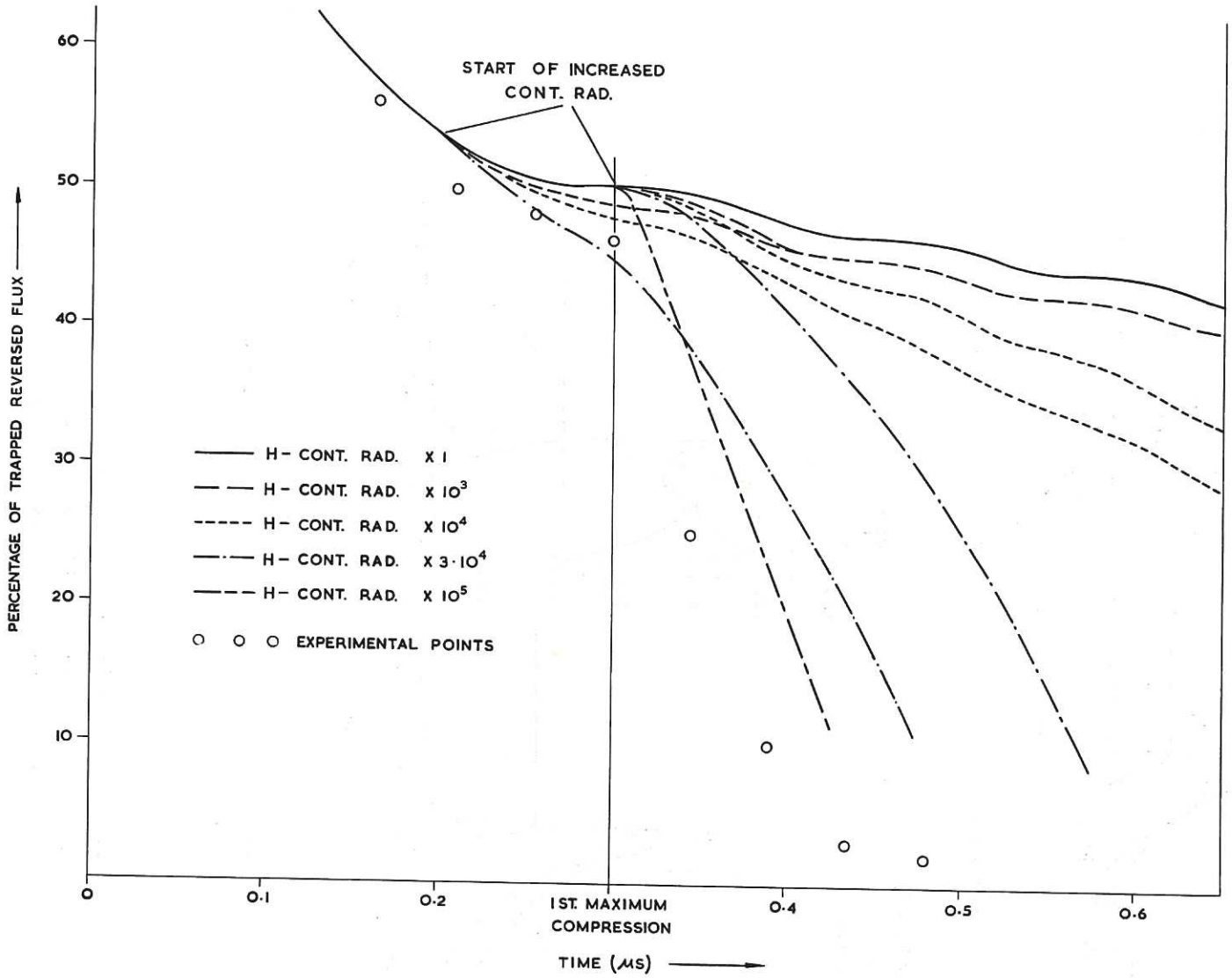

CLM-P47 Fig. 7

Numerical calculations showing how suddenly increasing the hydrogenic continuum radiation affects the decrease of trapped flux. Initial conditions: $p_o = 0.10$ torr, $T_o = 1.5$ eV, $B_{zo} = -1.8$ kG

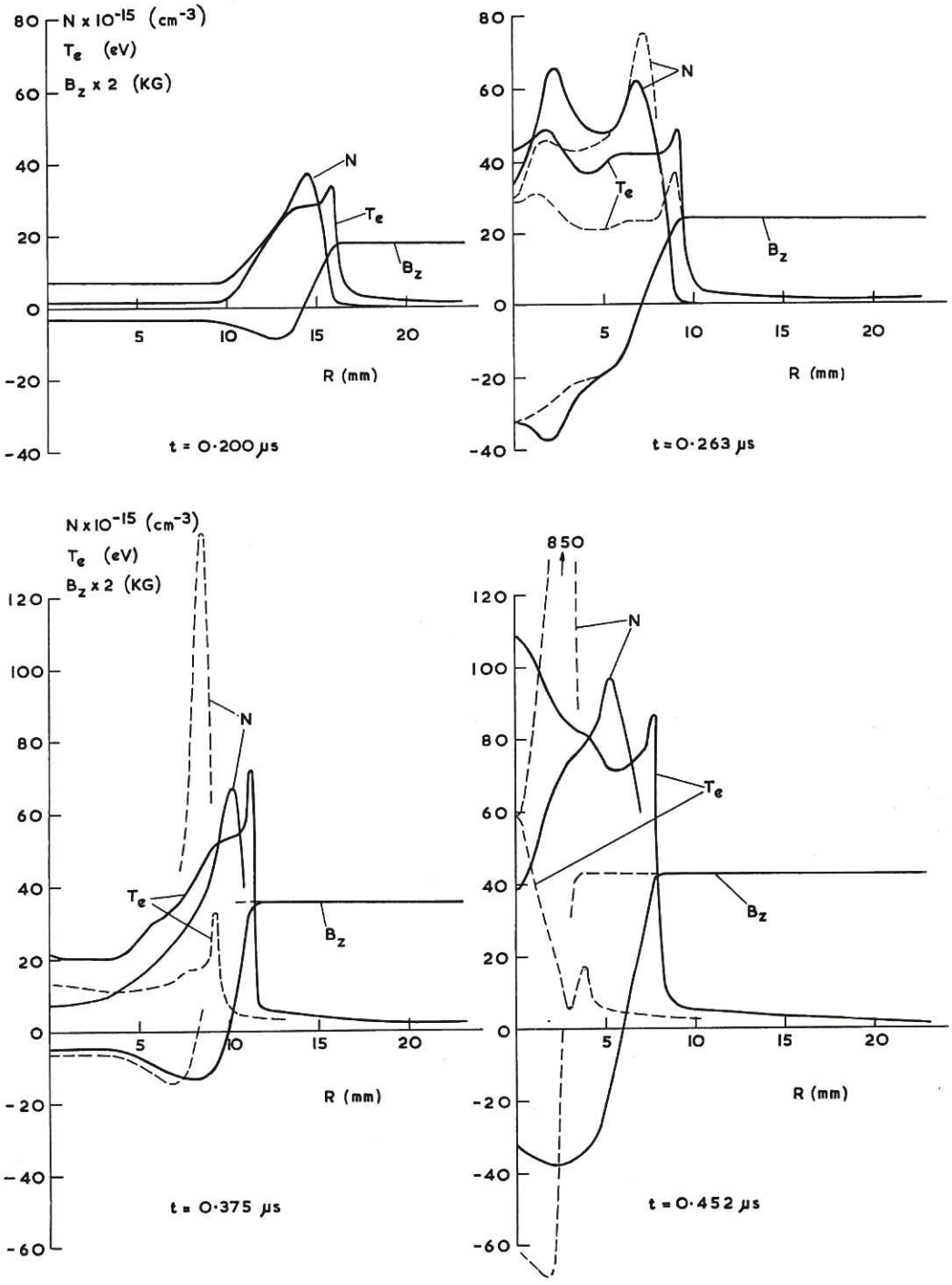

CLM-P 47 Fig. 8

Numerical calculations showing how suddenly increasing the hydrogenic continuum radiation affects the radial distributions of electron temperature, T_e, density, N, and magnetic field, B_Z. Initial conditions: $p_o = 0.10$ torr, $T_o = 1.5$ eV, $B_{zo} = -1.8$ kG